MICROSTRUCTURAL EVOLUTION IN DIFFUSE GRANULAR FAILURE: FORCE CHAINS AND CONTACT CYCLES

Antoinette Tordesillas
Department of Mathematics and Statistics, University of Melbourne, Melbourne, Australia

Luc Sibille
GeM Laboratory – University of Nantes, ECN, CNRS – Nantes, France

Sebastian Pucilowski
Department of Mathematics and Statistics, University of Melbourne, Melbourne, Australia

François Nicot
CEMAGREF – Unité ETNA – Grenoble, France

Félix Darve
3S-R Laboratory – INPG, UJF, CNRS – Grenoble, France

ABSTRACT: *We focus on structural evolution inside a deforming granular material, in three-dimensions, undergoing the so-called diffuse failure, i.e. failure in the absence of strain localization. We uncover and characterize quantitatively the basic building blocks for self-organization, enabling comparisons of the material's rheology to those recently reported for dense materials undergoing localized failure. The building blocks consist of: (i) the quasi-linear, load-bearing force chains, and (ii) their supporting network of contacts, the minimal n-cycles. Our preliminary study shows that, similar to localized failure, self-organization in the system gives rise to major load-bearing, columnar force chains which are supported laterally by truss-like 3-cycles. Under continued loading, the force chains ultimately fail by buckling, precipitating a catastrophic collapse of the material. However, unlike localized failure, the buckling events uncovered here do not appear to be localized.*

1 Introduction

The recent decades have witnessed remarkable strides in uncovering the "inner workings" of granular materials – with considerable insights derived from high-resolution experiments and discrete element (DEM) simulations (e.g. Iwashita & Oda 2000; Majmudar & Behringer 2005; Rechenmacher 2006; Desrues & Viggiani 2004; Tordesillas & Muthuswamy 2009; Walker & Tordesillas 2010; Tordesillas et al. 2010a, 2010b, 2011; Arevalo et al. 2010, and references cited therein). In particular, much light has been cast on the microscale mechanisms and underpinning dynamics behind the onset of instability and failure of granular materials via strain-localization. But equally important to geomechanics are non-localized diffuse modes of failure (Darve et al. 2004, 2007; Nicot & Darve 2007; Nicot et al. 2009; Sibille et al. 2008), and yet there is a dearth of knowledge on the micromechanics of diffuse failure. Detailed consideration of both modes of failure presents a broad gamut of questions for exploration that bears the potential to advance our understanding of granular failure to a whole new level. Such questions include: How and

why does a material favour one mode over the other? What are the fundamental commonalities and differences between localized and diffuse modes in terms of force transmission? In this joint study, we examine using Complex Networks the development of diffuse failure from the standpoint of force transmission, with particular attention paid to the force chains and their supporting contact cycles – key self-organized load-bearing structures whose cooperative behaviour was first examined in Tordesillas et al. 2010a.

Data used are from discrete element simulations of proportional strain loading paths on a three-dimensional dense granular assembly (Darve et al. 2007). These loading paths are rather unique and offer an opportunity for us to explore novel rheological granular behaviour that are not otherwise possible in traditional tests. These loading paths can be seen as a generalization of the undrained compression test. Diffuse failure is triggered from stress states reached along these proportional strain paths, and located inside the Mohr-Coulomb limit condition, by adopting an appropriate mixed (stress-strain) mode of control (Darve et al. 2004, 2007; Nicot et al. 2009). Although these simulations have been reported on in the past, the concepts and methods employed here constitute a first-of-a-kind approach for studies of diffuse failure in dense granular systems. Here we employ a Complex Systems approach, and analyze the quasi-statically deforming material as an evolving complex network (Walker & Tordesillas 2010; Tordesillas et al. 2010b). Our objective is to identify the basic building block structures for self-organization, study their evolution, and establish some common features with the structural evolution recently uncovered for localized failure (Tordesillas et al. 2010a, 2010b, 2011).

The paper is arranged as follows. We first describe the Discrete Element (DEM) simulation in Section 2. Therein we highlight salient features of the loading program to provide some insight into the loading conditions to which the specimen has been subjected, and thereby render more transparent the connection between such conditions and the material's response. The studies discussed in the Section 3 characterize this connection from the standpoint of the building-blocks for self-organization. We conclude in Section 4 with a summary of our key findings and highlight future research directions.

2 Discrete numerical simulations

2.1 The discrete element model

The three-dimensional numerical model (Darve et al. 2007; Sibille et al. 2009) is based on the discrete element method (Cundall & Strack 1979). It consists of a cubical shape assembly of more than 10,000 polydisperse spherical particles. The inter-particle interaction is modelled in the normal contact direction by a linear elastic relation, and in the tangential direction by an elastic perfectly plastic relation. The macroscopic stress-strain state of the granular assembly is imposed through six frictionless walls whose positions are controlled to follow the prescribed loading programme. The strain state is determined from wall positions and the stress state from wall-particle contact forces.

2.2 Loading programme and macroscopic response

The loading programmme (Darve et al. 2007) followed during simulations can be split into two steps. First, the numerical sample is brought from an isotropic stress-strain state to a given mechanical state denoted 'initial state'. Second, from this initial state, the loading programme is changed in order to try to trigger the failure of the sample.

In the first step, the sample is fully strain controlled. It means that the three principal strain components (ε_1, ε_2 and ε_3) are controlled and imposed by the operator, whereas the three principal stress components (σ_1, σ_2 and σ_3) constitutes the response parameters resulting from simulations. However, all strain components are not controlled directly, but some of the strain components are controlled trough a linear combination of them. For instance, for an isochoric compression with respect to axis '1' and with an axisymmetric condition ($\Delta\varepsilon_2 = \Delta\varepsilon_3$), the operator controls directly the parameter ε_1 by imposing $\Delta\varepsilon_1 > 0$ (i.e. a positive strain rate). In addition, to impose the isochoric condition, the operator imposes the following linear combination: $\Delta\varepsilon_v = \Delta\varepsilon_1 + 2\Delta\varepsilon_3 = 0$. In this paper, the isochoric loading programme is generalized by imposing always directly the axial strain $\Delta\varepsilon_1 > 0$, but by generalizing the linear combination imposed between principal strain components in the following way (Darve et al. 2004):

$$\Delta\varepsilon_1 + 2\,R\,\Delta\varepsilon_3 = 0 \tag{1}$$

where R is a parameter chosen by the operator. For $R = 1$ we retrieve the isochoric condition, while for $0 < R < 1$ the path is dilatant and for $R > 1$ it is contractant. A such loading programme is named 'proportional strain loading path'. Fig 1a shows the proportional strain path followed with the discrete element model for $0.7 \leq R \leq 1$.

Besides, if each strain component are controlled directly (and separately) the associated response parameters are the stress components respectively (i.e. in axisymmetric condition, ε_1 is associated with σ_1, and ε_3 with σ_3). The sum of the products between associated control and response parameters is homogeneous to an energy density W, writing in axisymmetric condition:

$$W = \varepsilon_1\sigma_1 + 2\,\varepsilon_3\sigma_3 \tag{2}$$

Nevertheless, for the proportional strain loading programme the control parameters are ε_1 and $\varepsilon_1 + 2\,R\,\varepsilon_3$. Consequently, the corresponding response parameters are no more σ_1 and σ_3 but rather $\sigma_1 - \sigma_3/R$ and σ_3/R respectively, in order to verify:

$$W = \varepsilon_1\sigma_1 + 2\varepsilon_3\sigma_3 = \varepsilon_1\left(\sigma_1 - \frac{\sigma_3}{R}\right) + (\varepsilon_1 + 2R\varepsilon_3)\frac{\sigma_3}{R} \tag{3}$$

Therefore, the computed responses to proportional strain loading paths displayed in Fig 1a should be represented in a $\sigma_1 - \sigma_3/R$ versus ε_1 diagram, as shown in Fig 1b.

Darve et al. 2004 and Nicot & Darve 2007 shown that bifurcation points, from which diffuse failure can develop (if proper conditions with respect to the loading direction and the mode of control of the sample are verified), can be detected by the vanishing of the second-order work. For proportional strain paths, since the relation $\Delta\varepsilon_1 + 2\,R\,\Delta\varepsilon_3 = 0$ is imposed, the second-order work $W2$ simplifies in the following way:

$$W2 = \Delta\varepsilon_1\left(\Delta\sigma_1 - \frac{\Delta\sigma_3}{R}\right) + (\Delta\varepsilon_1 + 2R\Delta\varepsilon_3)\frac{\Delta\sigma_3}{R} = \Delta\varepsilon_1\left(\Delta\sigma_1 - \frac{\Delta\sigma_3}{R}\right) \tag{4}$$

In addition, the operator also imposed the condition $\Delta\varepsilon_1 > 0$, consequently the sign of the second-order work is the same as the sign of $\Delta\sigma_1 - \Delta\sigma_3/R$. For R values sufficiently small (i.e. for strain paths sufficiently dilatant), $\sigma_1 - \sigma_3/R$ *vs* ε_1 curves in Fig 1b present a peak. At the peak of $\sigma_1 - \sigma_3/R$, the second-order work vanishes and then takes negative values along the following decreasing curves.

The mechanical states corresponding to these maximum of $\sigma_1 - \sigma_3/R$ and the following decreasing curves (i.e. corresponding to nil or negative values of W2) constitute mixed limit

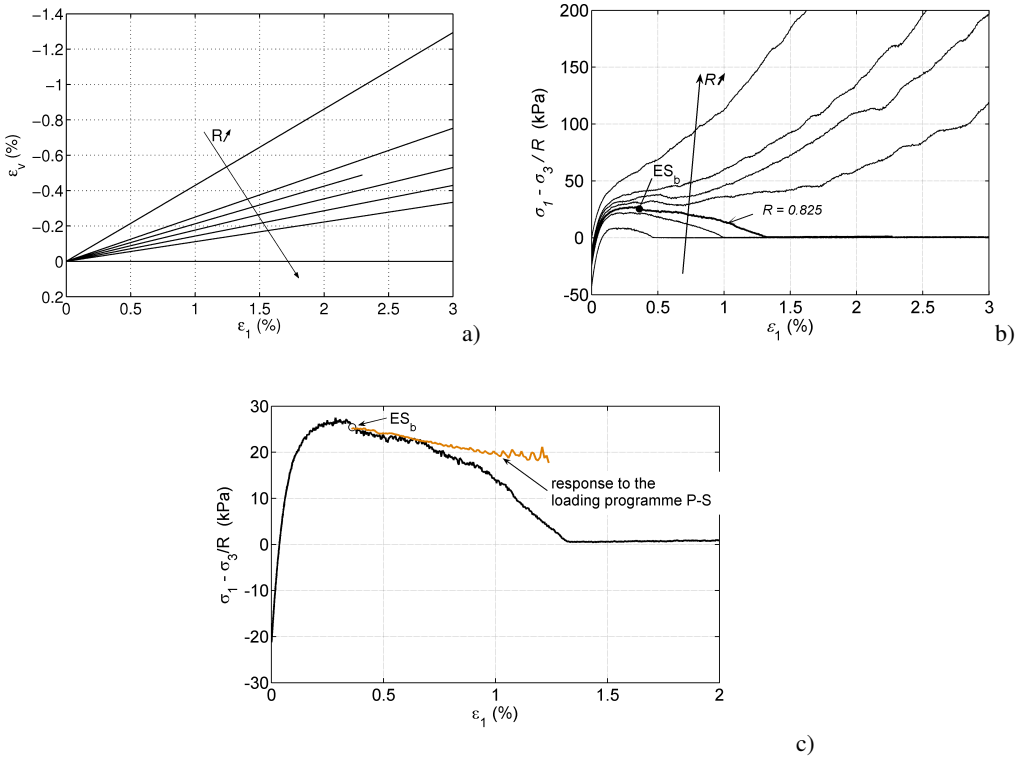

Fig. 1. a) Proportional strain loading paths applied to the sample for $R = 0.7$; 0.8; 0.825; 0.85; 0.875; 0.9; 1.0; b) computed responses; c) computed response to the proportional strain path for $R = 0.825$, and computed response to the loading programme P-S.

states (Darve et al. 2004). These mixed limit states can been seen as a generalization of classical limit stress states. Here the considered limit states are mixed because they cannot be crossed for a mixed stress-strain control mode. Therefore, the first loading programme fully strain controlled is now, in a second step, changed by a mixed loading programme (partially defined with strain components and stress components respectively) in order to try to trigger failure. We need to impose a mixed mode of control, by still imposing the strain loading direction defined by equation (1) (Darve et al. 2004), together with forcing the sample to cross the mixed limit state considered. As the response parameter $\sigma_1 - \sigma_3/R$ decreases when the sample is loaded from a mixed limit state, we simply invert the control and response parameters ε_1 and $\sigma_1 - \sigma_3/R$, in order to impose an increase of $\sigma_1 - \sigma_3/R$.

To resume, we consider now only the proportional strain loading path characterized by $R = 0.825$, the corresponding computed response path is identified in Fig 1b and c. Along this response path we consider the stress-strain state denoted ES_b in Fig 1b and c, and located slightly after the peak of $\sigma_1 - \sigma_3/R$. This state is a mixed limit state and it will constitute the initial state for the new loading programme, denoted P-S, and consisting to impose together to the sample:

$$\Delta\varepsilon_1 + 2R\Delta\varepsilon_3 = 0 \tag{5}$$

and

$$\Delta\sigma_1 - \Delta\sigma_3/R = 250 \text{ Pa} \quad \text{(representing 1 \% of } \sigma_1 - \sigma_3/R \text{ at } ES_b) \tag{6}$$

with $R = 0.825$.

Fig 2 presents the computed response to the loading programme P-S: actually the small increase in $\sigma_1 - \sigma_3/R$ that is tried to be applied cannot be reached together with the imposed condition $\Delta\varepsilon_1 + 2R\Delta\varepsilon_3 = 0$ (see also Fig 1c). In addition the stress components σ_1 and σ_3 tend

to vanish with a sharp temporal increase of strains and kinetic energy (Nicot et al. 2009) of the sample (i.e. the sum of the kinetic energy of all particles of the assembly), illustrating the sudden failure of the sample (loss of controllability in the sense of Nova 1994) characterized by a transition from a quasi-static regime to a dynamic regime (Darve et al. 2007; Nicot et al. 2009), where inertial terms are no more negligible (explaining why the axial stress σ_1 does not vanish while $\sigma_3 = 0$ at the end of the simulation). These results show that ES_b is actually a mixed limit state that cannot be passed according to the mixed loading programme P-S, resulting in the diffuse failure of the sample. From Fig 2, and more particularly from the change of kinetic

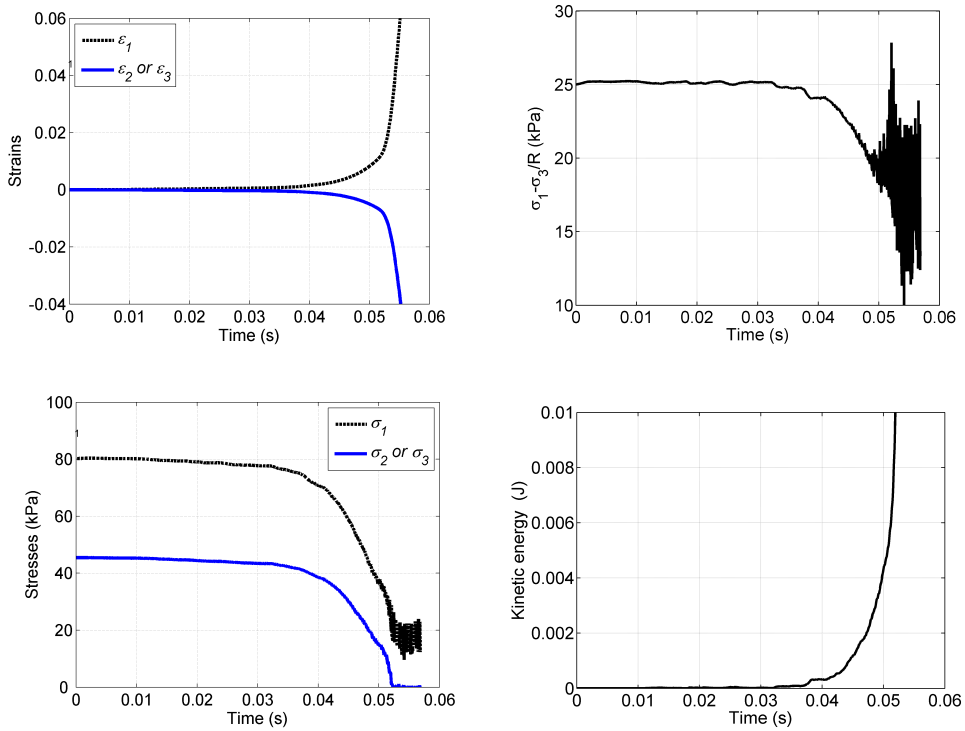

Fig. 2. Failure of the granular assembly simulated from the mixed limit state ES_b, resulting of the application of the mixed stress-strain loading programme P-S

energy, two different response regimes can be identified, firstly an almost stable and quasi-static regime followed by an unstable and dynamic regime. Table 1 give time intervals of these regimes which will be investigated in Sec 3.

Table 1. Time intervals (s) of key regimes.

Initial state	Loading programme	Stable–quasi-static	Unstable–dynamic
ES_b	P-S	$(0.0, 0.03)$	$(0.03, 0.06)$

3 Building blocks for self-organization

The process of self-organization during granular deformation presents hallmarks of complexity that are more directly tractable compared to other well-known complex systems, e.g. telecommunication, social and biological networks (Walker & Tordesillas 2010; Arevalo et al. 2010; Watts & Strogatz 1998). Complexity in granular materials emerges from the interactions of the constituent particles through their contacts: the contacts can be tracked in real time and the interactions between particles can be quantified through the forces and torques transmitted through these contacts. Other complex networks do not lend themselves so readily to this level of quantitative detail: interactions between computers or human beings or protein molecules are difficult to define, let alone measure (Watts & Strogatz 1998).

We have full information on contacts for the system described in Sec 2. Thus we can construct a complex network (or mathematical graph) comprising nodes and links, to represent the sample at every fixed simulation time or strain state of the loading history. The nodes in the network represent the particles, while the links connecting the nodes in the network represent the contacts between particles in the system. We first identify the load-bearing quasi-linear structures of m-force chains and their supporting cyclic network of contacts, the minimal n-cycles, where $m \geq 3$ and $n \geq 3$ are integers representing the number of particles that form the chain or cycle (Tordesillas et al. 2010a, 2011). We refer readers to Tordesillas et al. 2011 for details of the methods and algorithms used to identify force chains and minimal n-cycles, from the particle scale information that forms the output data of the DEM simulation described in Sec 2. At any given strain state in the simulation, a columnar force chain is confined by supporting contacts that can be succinctly summarised by the minimal cycle basis of the contact network, i.e. n-cycles, so that each force chain will have its own set of minimal cycles of various sizes n (see Fig 3). In this context, force chains are distinct from n-cycles in that force chains are physical structures made up of m particles, whereas cycles are made up of contacts and n is the number of particles that form the contact cycle. The smallest members of the n-cycles, i.e. 3-cycles, are special from the standpoint of packing and network connectivity: they are formed from three particles in mutual contact, and thus exemplify a densely packed and tightly connected structure that frustrates rotations (Tordesillas et al. 2010a). More generally, rotations are 'frustrated' in groups of particles forming an odd-cycle, whereas $even$-cycles allow free rotations (akin to the action of ball bearings) (Tordesillas et al. 2010a, 2011). Since particle rotations have long been identified as playing a crucial role in the deformation of granular materials – especially in the failure regime – the odd-cycle membership can be reasonably expected to play a key role in the mobilization of shear strength or resistance to applied loads.

Past experimental and numerical studies of dense granular materials undergoing localized failure, in both two and three dimensions, have shown that force chains and their surrounding contact cycles may be viewed as the basic building blocks for self-organization, and their collective and cooperative interactions govern global rheology (Tordesillas et al. 2010a, 2010b, 2011, 2010c). For the sample under study, we find the distributions of the populations of n-force chains in Fig 4 to be qualitatively similar to those for systems that undergo localized failure. The relative dominance of a given class of n-force chains decreases as n grows. The shortest, 3-force chains constitute the clear majority. From a structural mechanics standpoint, this makes sense: like solid columns, we can expect that, with all else equal, a short column would be more stable than a long column. Indeed in a recent study of force chains (Tordesillas et al. 2011), the 3-force chains proved to be the most stable in the system, although the inverse correlation between stability and length rapidly weakens for high values of n ($n > 4$). This is because the more particles

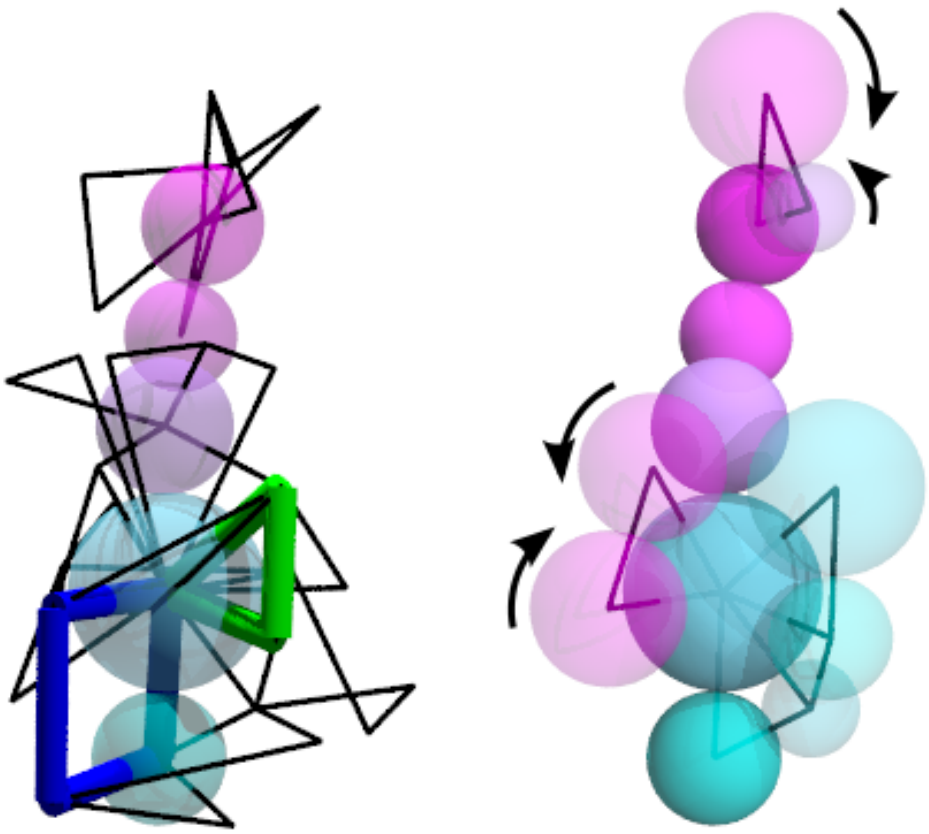

Fig. 3. *Left:* A 5-force chain in the sample and its local n-cycle membership: five 3-cycles, five 4-cycles, seven 5-cycles, two 6-cycles and one 7-cycle. A 3-cycle and 4-cycle have been highlighted to aid visualization. *Right:* The same force chain is shown with only its 3-cycles and neighbouring particles which form these cycles. An example mode of rotation in the confining neighbours of the force chain is shown in two of the 3-cycles: irrespective of the rotational direction of the force chain particle, rotation will be frustrated in one contact. This frustration prevails for all possible directional combinations in the particles' rotations.

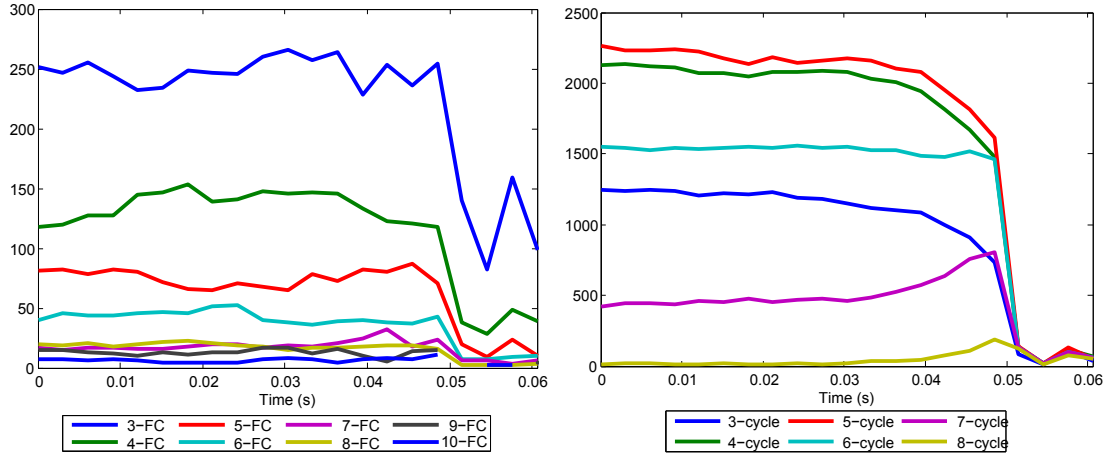

Fig. 4. Evolution of the populations of various classes of: (*left*) force chains, m-FC, and (*right*) n-cycles throughout loading.

there are in the chain, the more variations of the contributors to stability (e.g. distribution of the magnitude and topology of the lateral forces) become possible, effectively obscuring the isolated influence of length. By contrast, the distributions of the n-cycles in Fig 4 differ markedly with those for a system which fails in the presence of localization. In the latter case, the relative dominance of n-cycles decreases as their size grows, similar to the population distributions of force chains. The population in each class of n-cycle is close to being constant prior to the simulation time of 0.03. From times 0.03 to 0.04, the n-cycle populations decrease steadily but slowly for the dominant classes $n = 3, 4, 5$, while classes $n = 7, 8$ see a small increase in numbers. From times 0.04 to 0.05, we see a marked increase in the rate of population decline in the n-cycles, followed by a sudden and precipitous drop for all (except for $n = 8$) at just after the time of 0.05 – the same time that most of the force chains in the system collapse. The trends in the behaviour of the building blocks are consistent with the macroscopic stresses reported in Sec 2.

Similar to localized failure, we also observe cooperative interactions between the force chains and 3-cycles. The former resides in local neighbourhoods with not just higher concentrations of contacts per particle, but also a relatively higher number of 3-cycles per particle (Fig 5). In other words, force chains favour more contacts and prefers these contacts to be in 3-cycle formation. These truss-like 3-cycles have been shown in recent studies to provide dual support to force chains: they frustrate particle rotations (rotations being integral to buckling), and prop-up the force chain during buckling. We also considered the strongest 3-cycles, i.e. 3-force-cycles, in which *each* contact bears above the global average force (Tordesillas et al. 2010a). In earlier work (Tordesillas et al. 2010a), these strong 3-force-cycles were found to emerge at the time and locale of greatest need, i.e. during and in the region of strain localization where the buckling force chains are confined. In the sample under study, the 3-force-cycles appear to be spread throughout the sample (data not shown).

Overall, the common feature that this sample shares with systems undergoing localized failure is the reliance of load-bearing columnar force chains on the support of 3-cycles. That said, despite the material self-organizing to provide the force chains with stabilizing 3-cycles, the continued loading of the system ultimately 'wins': force chains eventually reach their load-carrying capacity and collapse by buckling as evident in times from 0.04 in Fig 6. Compare this to the preceding degradation of the supporting 3-cycles which commences at around the time of 0.02 onwards in Fig 4 and around the time of 0.03 onwards in Fig 5. The consequent collective buckling of force chains, in turn, precipitates the total collapse of the sample (Fig 6). Unlike in localized failure where the buckling is localized in distinct zones, here the buckling appears to be widespread and non-localized (Fig 6). Ongoing studies are focussed on a quantitative analysis of the spatio-temporal distributions of the buckling force chains and 3-force cycles in specimens undergoing diffuse failure, to determine whether the spread of these important mesoscopic structures throughout the material is indeed realised.

4 Conclusion

We examined self-organization in a sample undergoing diffuse failure. Quasi-linear and cyclic building blocks of force chains and their surrounding n-cycles, respectively, were identified. The evolution of these building blocks is consistent with the global measures of stress. There is evidence of cooperative evolution that elucidates *functional* behaviour among the building blocks. Truss-like 3-cycles laterally support column-like force chains, just as they do for systems that fail through strain localization. Despite the stabilizing benefits provided by the 3-cycles, columnar force chains are prone to fail by buckling. Ultimately, the collective buckling of these major

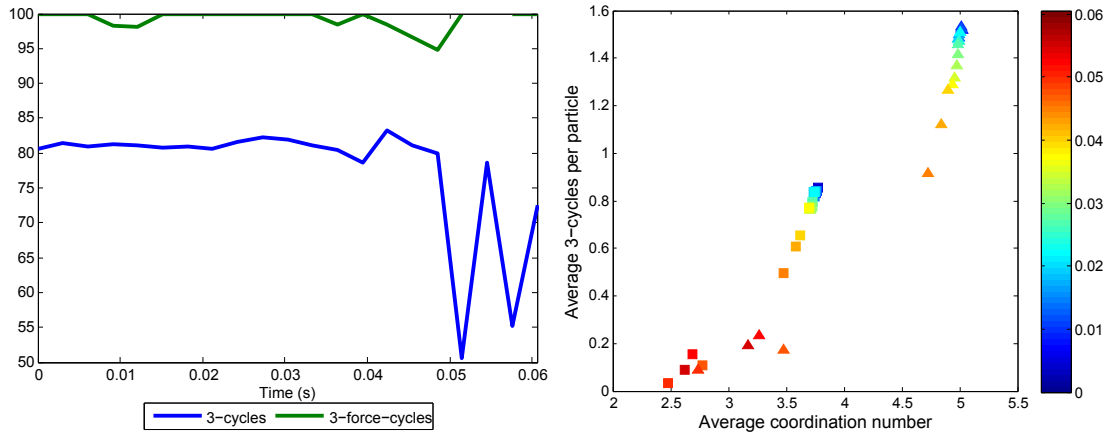

Fig. 5. (*Left*) Percentages of 3-cycles and 3-force cycles laterally supporting force chains (FCs) throughout loading. (*Right*) The evolution of the average number of contacts per particle (coordination number) and average number of 3-cycles per particle, for two subsets of the sample, i.e. those particles in force chains (△) versus the rest (□). Legend indicates simulation time.

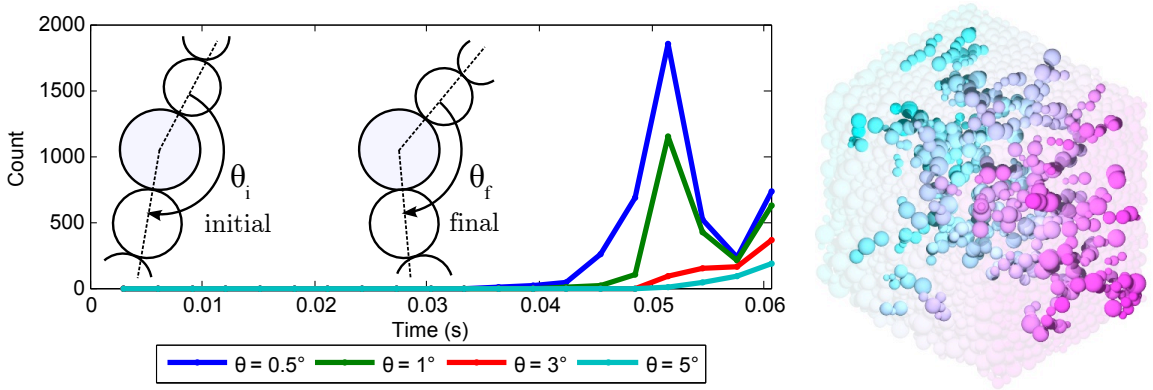

Fig. 6. (*Left*) The number of particles in buckling force chains which buckle by no less than the threshold value of θ, $\theta_b \geq \theta$, for one time step in the simulation. *Inset* illustrates the buckling angle $\theta_b = \theta_i - \theta_f$. (*Right*) Buckling force chains at simulation time of 0.0606, where $\theta_b \geq 1.0^\circ$: a total of 627 particles are in this set.

load bearing structures precipitate the collapse of the sample. Prima facie evidence suggests that the buckling of force chains are spread throughout the sample. These preliminary results provide impetus for a detailed investigation into the evolution of force chains and their minimal contact cycles, in particular, one aimed at uncovering the precise details of cooperative behaviour between them, so that we can better understand the underlying decision-making process that the material employs as it deforms under load.

REFERENCES

Arevalo, R., Zuriguel, I., & Maza, D. (2010). Topology of the force network in the jamming transition of an isotropically compressed granular packing. *Physical Review E 81*, 041302.

Cundall, P. & Strack, O. (1979). A discrete numerical model for granular assemblies. *Geotechnique 29*(1), 47–65.

Darve, F., Servant, G., Laouafa, F., & Khoa, H. (2004). Failure in geomaterials : continuous and discrete analyses. *Computer Meth. Appl. Mech. Eng. 193*(27-29), 3057–3085.

Darve, F., Sibille, L., Daouadji, A., & Nicot, F. (2007). Bifurcations in granular media : macro- and micro-mechanics approaches. *Comptes Rendus Mécanique 335*(9-10), 496–515.

Desrues, J. & Viggiani, G. (2004). Strain localization in sand: an overview of the experimental results obtained in grenoble using stereophotogrammetry. *Int. J. Num. Anal. Methods Geomech. 28*, 279–321.

Iwashita, K. & Oda, M. (2000). Micro-deformation mechanism of shear banding process based on modified distinct element method. *Powder Technology 109*, 192–205.

Majmudar, T. & Behringer, R. (2005). Contact force measurements and stress-induced anisotropy in granular materials. *Nature 433*, 1079–1082.

Nicot, F. & Darve, F. (2007). A micro-mechanical investigation of bifurcation in granular materials. *Int. J. of Solids and Structures 44*, 6630–6652.

Nicot, F., Sibille, L., & Darve, F. (2009). Bifurcation in granular materials: An attempt for a unified framework. *Int. J. of Solids and Structures 46*, 3938–3947.

Nova, R. (1994). Controllability of the incremental response of soil specimens subjected to arbitrary loading programmes. *J. Mech. behav. Mater. 5*(2), 193–201.

Rechenmacher, A. (2006). Grain-scale processes governing shear band initiation and evolution in sands. *J. Mech. Phys. Solids 54*, 22–45.

Sibille, L., Donzé, F., Nicot, F., Chareyre, B., & Darve, F. (2008). From bifurcation to failure in a granular material, a dem analysis. *Acta Geotechnica 3*(1), 15–24.

Sibille, L., Nicot, F., Donzé, F., & Darve, F. (2009). Analysis of failure occurrence from direct simulations. *European Journal of Environmental and Civil Engineering 13*, 187–201.

Tordesillas, A., Lin, Q., Zhang, J., Behringer, R., & Shi, J. (2011). Structural stability and jamming of self-organized cluster conformations in dense granular materials. *J. Mech. Phys. Solids 59*, 265–296.

Tordesillas, A. & Muthuswamy, M. (2009). On the modelling of confined buckling of force chains. *Journal of Mechanics and Physics of Solids 57*, 706–727.

Tordesillas, A., O'Sullivan, P., Walker, D., & Paramitha (2010b). Evolution of functional connectivity in contact and force chain networks: feature vectors, k-cores and minimal cycles. *Comptes rendus mecanique, CRAS (Proceedings of the French Academy of Sciences) 338*, 556–569.

Tordesillas, A., Pucilowski, S., Walker, D., Peters, J., & Hopkins, M. (2010c). A complex network analysis of granular fabric evolution in three-dimensions. *Dynamics of Continuous, Discrete and Impulsive Systems, Series B*. in press.

Tordesillas, A., Walker, D., & Lin, Q. (2010a). Force cycles and force chains. *Physical Review E 81*, 011302.

Walker, D. & Tordesillas, A. (2010). Topological evolution in dense granular materials: A complex networks perspective. *Int. J. Solids Struct. 47*, 624–639.

Watts, D. & Strogatz, S. (1998). Collective dynamics of 'small-world' networks. *Nature 393*, 440–442.